Korean J. Chem. Eng., **28**(3), 770-777 (2011)
DOI: 10.1007/s11814-010-0415-0

Air gap membrane distillation on the different types of membrane

Ke He, Ho Jung Hwang, and Il Shik Moon†

Department of Chemical Engineering, Sunchon National University, 315 Maegok dong, Suncheon, Jeonnam 540-742, Korea
(*Received 12 November 2009 • accepted 28 August 2010*)

Abstract−Seawater desalination through the air gap membrane distillation (AGMD) process shows merit for its ambient operational conditions and low energy consumption. In this paper nine types of commercially available membranes were characterized to understand the membranes more comprehensively. The density, porosity, mean pore radius, liquid entry pressure (LEP), and contact angle (CA) of the membranes were determined. AGMD experiments were performed for the membranes to investigate the membrane difference on permeation flux and salt rejection. The effects of operating parameters such as temperature, flow rate, and NaCl concentration were studied. The 0.22 μm pore size PTFE membrane showed excellent performance for its higher permeability and higher hydrophobicity than other membranes. The mass transfer coefficients for three types of PTFE membranes were calculated from the results of the experiments.

Key words: Air Gap Membrane Distillation, Seawater Desalination, PTFE Membrane, Gas Permeability, LEP

INTRODUCTION

Fresh water is becoming increasingly scarce worldwide, and it is commonly expected that the demand for drink water will be increased drastically in the near future. Providing fresh water is an important issue for most nations. It would be attractive to explore the possibility of desalinating seawater to overcome the water-shortage [1].

Desalination can be achieved by a number of techniques. The processes require significant quantities of energy to achieve separation of salts from seawater. Current commercially available desalination technologies can be classified into i) phase change or thermal process, and ii) membrane or single-phase processes [2]. Membrane distillation (MD) is an emerging alternative technology for separation of liquids. By using MD, pure water can be extracted from the aqueous solutions through a hydrophobic microporous membrane when a vapor pressure difference is established across the membrane. A hydrophobic membrane can inhibit the permeance of water by membrane surface tension but allow the passage of vapor. Therefore, the water vapor will be able to pass from the higher vapor pressure to the lower vapor pressure sides. Since the 1980's, along with the rapid development of advanced membrane preparation techniques and low energy consumption for the separation, the membrane distillation process has gained renewed attention worldwide.

The main application of the MD process is the production of ultrapure water [3], from desalination of brackish sea water and highly saline water [4,5] and successfully applied to the concentration of several non-volatile solutes in aqueous solutions like salt, sugar, fruit juices, blood, and waste water treatment, etc. [6]. In recent years, the MD process has also been proposed as a separation technique for ethanol from aqueous solution [7,8], breaking of azeotropic mixtures [9], concentrating of the various acids [10-12], and separation of isotopic water [13].

One requirement for the MD process is that the membrane must be unwetted and only vapor is present within its pores. To avoid membrane wetting, the surface tension of the liquid in direct contact with membrane should be large and the surface energy of the membrane material should be low. Whether the membrane is wetted is associated with such factors as the liquid entry pressure (LEP). Below LEP, the hydrophobicity of the membrane cannot sustain water from entering its pores. The relationship of LEP with pore size, liquid-solid contact angle and liquid surface tension can be expressed by Cantor equation. Therefore, a membrane with large pore size has relatively lower LEP, which indicates that it is more easily wetted during operation.

$$\mathrm{LEP}=\frac{2\mathrm{X}\sigma\cos\theta}{\mathrm{r}} \text{ and } \mathrm{lowLEP}=\frac{2\mathrm{X}\sigma\cos\theta}{\mathrm{r}_{max}} \tag{1}$$

where X is a geometric factor determined by pore structure, σ is the surface tension of the liquid, θ is the liquid-solid contact angle, and r is the membrane pore radius.

Depending on the collections of the permeate, mass transfer mechanisms through the membrane and the generations of driving force, MD systems may be classified into four different categories: direct-contact MD (DCMD), air gap MD (AGMD), sweeping gas MD (SGMD), vacuum MD (VMD) and osmotic MD (OMD). The present work is focused on the AGMD applications. A schematic diagram of the AGMD membrane module is shown in Fig. 1. In the AGMD process, separation of the solutions is determined by the liquid-vapor interfacial conditions at the feed side and by the differences in their diffusion/convection rates across the membrane and the air-gap [14-17]. The main advantage of AGMD is considerable reduction of the heat loss caused by conduction through the membrane. Since the permeate can be obtained directly on a air gap layer rather than mixed in a cold fluid such as DCMD, it is easy to decide whether there is membrane leakage or wetting occurring by analyzing the permeate composition. On the other hand, compared with

†To whom correspondence should be addressed.
E-mail: ismoon@sunchon.ac.kr

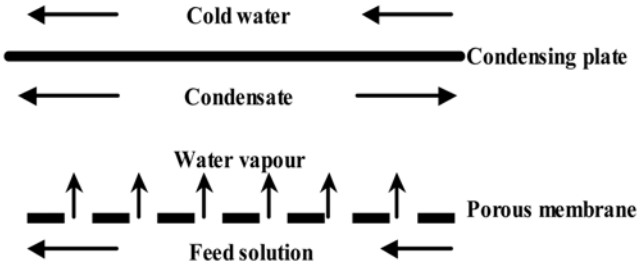

Fig. 1. Schematic diagram of AGMD membrane module.

other MD processes, the product of AGMD can be weighted accurately.

Many researchers have attempted to apply the AGMD to desalination of seawater in different applications [11,17-19]. Walton et al., using low grade thermal energy supplied by a salt gradient solar pond, tested the desalination of brine using the AGMD system [20]. In the studies the permeation flux reached a maximum of 6 L/m^{2}hr. Biner and Plantikow investigated solar powered membrane distillation using an AGMD module [21]. They observed in the pilot plant that the mass transfer resistance created by the air gap resulted in a large reduction in the trans-membrane water flux. Meindersma et al. [22] investigated the energy requirement and cost estimation of the desalination process using AGMD in the counter-current flow mode. Feng et al. [23] studied the production of drinking water from saline water by AGMD using polvinylidene fluoride nanofiber membrane. Chouikh et al. studied the AGMD and modified AGMD for desalination of seawater using hydrophobic membrane type [24]. However, the permeated flux in the modified AGMD was observed around 9 kg/m^{2}hr. Theoretical and experimental studies have been carried out on AGMD of different aqueous solutions by Liu et al. [25].

In this paper, nine types of commercially available membranes were characterized by gas permeability test, liquid entry pressure (LEP) test, and measurement of contact angle (CA) experiment. Then the membranes were used for the AGMD system to investigate the membrane difference on permeation flux and salt rejection. The effects of operating parameters such as temperature, flow rate, and NaCl concentration were studied. The mass transfer coefficient for PTFE 0.22 membrane was calculated from the results of the experiments.

EXPERIMENTAL

1. Reagents

All chemicals used in the experiments were of analytical reagent grade. The NaCl solution was prepared by using de-ionized water and pure NaCl (DAE JUNG chemical Co. Ltd.) with the concentrations in the ranges between 1% and 10%. The conductivity of the feed was measured with an EC meter (EC470-L, ISTEK, KOREA). The salt rejection was calculated according to the conductivity.

2. Membranes and their Properties

Nine types of flat sheet porous membranes made of PTFE, PVDF and PP materials with different pore sizes manufactured by Membrane Solutions (Shanghai, China) were used for the experiments. The characteristics of the membrane are given in Table 1. The membranes were soaked in the de-ion water for a minimum of 12 hours before being used in the AGMD apparatus.

Table 1. Characteristics of membranes provided by the manufacturer

Material	Pore size (μm)	Thickness (μm)	Support material	Diameter (mm)
PTFE	0.22	160±40	PP	142
PTFE	0.45	160±40	PP	142
PTFE	1.00	160±40	PP	142
PVDF	0.22	100±10	PET	142
PVDF	0.45	100±10	PET	142
PVDF	1.00	100±10	PET	142
PP	0.22	200±10	Unsupported	142
PP	0.45	200±10	Unsupported	142
PP	1.00	200±10	Unsupported	142

2-1. Density and Porosity

The membrane density was calculated by equation:

$$\rho = \frac{m}{v} \tag{2}$$

where m is the weight of membrane and v is the volume.

The membrane porosity, ε, is defined as the volume of the pores divided by the total volume of the porous membrane. It can usually be direct calculated by using apparent density method [26]:

$$\varepsilon = 1 - \frac{v_{polymer}}{v_{total}} = 1 - \frac{\rho_{membrane}}{\rho_{material}} \tag{3}$$

where $\rho_{membrane}$ is the density of the membrane and $\rho_{material}$ is the density of raw material.

2-2. Gas Permeability

A gas permeability experiment setup was built, and the effectiveness of the membrane was 0.00039 m^2. The equipment was made ready for the gas permeation test by filling the pressure vessel with nitrogen at a pressure of 5×10^3 Pa. Then the stainless steel membrane holder inlet valve was opened. The inlet nitrogen pressure was controlled with a pressure gauge. The flux of the nitrogen flowing from the bottom of the membrane was measured by a soap flow meter. In the present study, the permeation flux of nitrogen through each dry membrane was measured at various transfer membrane pressures, in the range of 5-200 kPa. The permeation of single gas

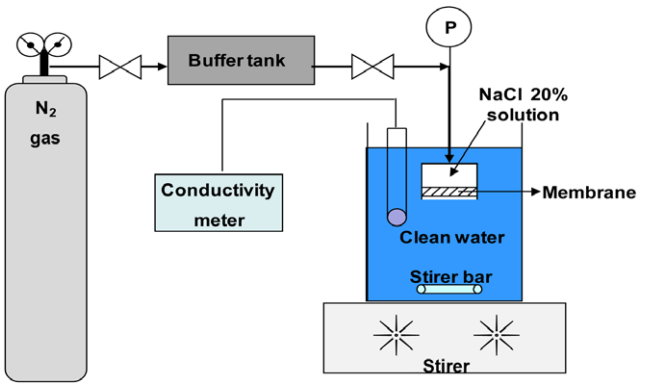

Fig. 2. Schematic diagram of the LEP experimental apparatus.

nitrogen driven by a total pressure across a porous membrane will be regulated by Knudsen diffusion-Poiseuille flow mechanism. The total mass flux can be obtained from the following equations:

$$N=\left(\frac{8}{3}\frac{\varepsilon r}{\tau\delta}\sqrt{\frac{1}{2\pi RMT}}+\frac{\varepsilon r^2}{\tau\delta}\frac{1}{8\eta}\frac{P_m}{RT}\right)\Delta P \quad \text{In other form: } J=A_0+B_0*P_m, \quad (4)$$

where $A_0=\frac{8}{3}\frac{\varepsilon r}{\tau\delta}\sqrt{\frac{1}{2\pi RMT}}$, $B_0=\frac{\varepsilon r^2}{\tau\delta}\frac{1}{8\eta}\frac{P_m}{RT}$, R is the gas constant, T is the absolute temperature, M is the molecular weight of the gas, r is the membrane pore radius, ε is the porosity, τ is the membrane tortuosity, δ is the membrane thickness, and P_m is the average pressure within the membrane pores. On this basis, the membrane characteristics can be obtained from A_o and B_o by the following equations:

$$r=\frac{16}{3}\frac{B_0}{A_0}\sqrt{\frac{8RT}{\pi M}}\eta \text{ and } \frac{\varepsilon}{\tau\delta}=\frac{8\eta RTB_0}{r^2} \quad (5)$$

2-3. Liquid Entry Pressure (LEP)

Fig. 2 shows a schematic diagram of measurement LEP values. The upper side of filtration cell was filled with 20% concentration of NaCl solution. The filtration cell was soaked in tank filled with pure water. A conductivity meter was used to check the pure water conductivity changes; then pressure was applied from the nitrogen cylinder on 20% concentration of NaCl solution. The pressure was increased until the NaCl solution penetrated through the membrane. At that moment, outside pure water conductivity will increase quickly. The pressure was recorded and considered as the LEP for the tested membrane sample. The experiment was done three times with three pieces of different sheets from different batches. The results were averaged to obtain the LEP.

2-4. Contact Angle (CA)

The contact angles for nine types of membranes were measured by using the SV Sigma 701 Tensiometer from KSV Instruments Limited, inland. The membrane was brought into contact with distilled water. The principle of this measurement is through the forces of interaction, geometry of the solid and surface tension of the liquid; the advancing contact angle was calculated by the aid of the computer software. Several readings were measured and an average was obtained from the results.

3. AGMD Experimental Setup

The experimental setup of the AGMD system is schematically depicted in Fig. 4. The setup consists of three compartments: the feed (bottom cell), the permeation (middle cell) and the cooling part (top cell). The compartments are made of high density polyethylene (HDPE) to resist corrosion by the NaCl solution. The feed NaCl solution flows through the bottom cell while the cooling water passes through one side of the condensing plate in the top cell. The permeate liquid is collected in the middle cell, which is placed between the feed and coolant compartment. The stainless steel grid is used as a membrane support to maintain the air gap space. The cooling plate is made of stainless steel. The AGMD system is horizontally installed. The feed and permeate are separated by a hydrophobic porous membrane. The actual effective area of the membrane is 0.01382 m^2.

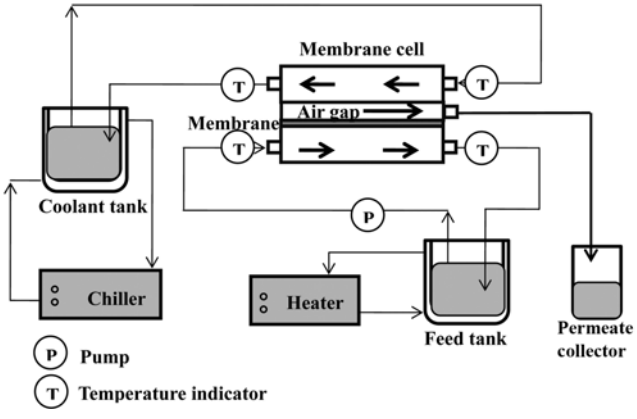

Fig. 3. Schematic diagram of AGMD experimental apparatus.

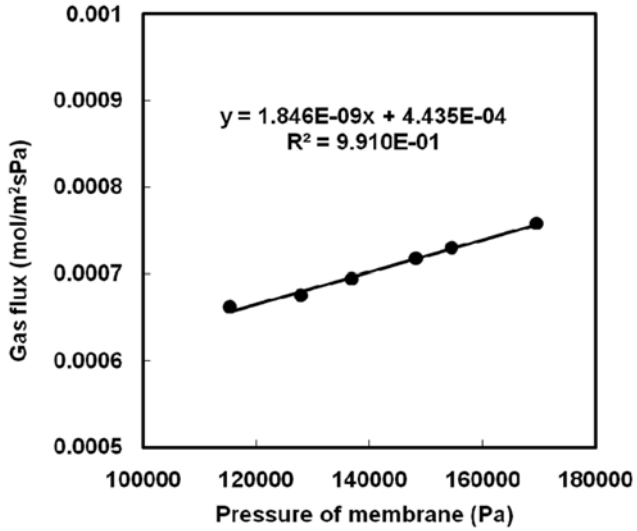

Fig. 4. The relationship of flux with P_m obtained from gas permeation experiment.

The feed is contained in a double walled reservoir and is circulated through the membrane module by using a variable flow peristaltic pump. The cooling water is maintained at the conditions: temperature of 15 °C, flow rate of 100 ml/min. The outlet temperatures of the hot side and coolant side were continually monitored. The permeated liquid was collected in a graduated cylinder, and the volumes were measured at regular time intervals. The purity of the water extracted was determined by the water conductivity using an electric conductivity meter.

RESULTS AND DISCUSSION

1. Membrane Characterization

1-1. Gas Permeability

As pointed out by many researchers, the requirements for MD membranes are good thermal stability and chemical stability, higher permeability, higher liquid entry pressure (insensitive hydrophobicity) and low heat conductivity. Hydrophobic microporous membranes made of polypropylene (PP), polytetrafluoroethylene (PTFE) and polyvinylidene fluoride (PVDF) are the commonly used membranes in MD.

Fig. 4 shows the gas permeability experimental result about the relationship of flux with P_m for PTFE 0.22 membrane under a con-

Table 2. Membrane characteristics of gas permeation test

Membrane	A_o	B_o	r (m)	$\varepsilon/\tau\cdot\delta$ (m^{-1})
PTFE0.22	4.44E-04	1.85E-09	1.73E-07	1.99E+04
PTFE0.45	5.08E-04	3.82E-09	3.12E-07	1.26E+04
PTFE1.00	4.18E-04	5.44E-09	5.41E-07	5.99E+03
PVDF0.22	1.12E-04	5.56E-10	2.06E-07	4.22E+03
PVDF0.45	2.26E-04	1.49E-09	2.73E-07	6.42E+03
PVDF1.00	2.59E-04	2.74E-09	4.40E-07	4.56E+03
PP0.22	7.09E-04	3.39E-09	1.99E-07	2.77E+04
PP0.45	1.11E-03	9.20E-09	3.46E-07	2.48E+04
PP1.00	7.62E-04	9.90E-09	5.40E-07	1.10E+04

stant pressure difference of 1 kPa. The data are correlated well with a straight line. In terms of the Eq. (4), the membrane characteristics can be obtained from the slope and the intercept of this line. For the PTFE 0.22 membrane, investigated A_o is 4.435×10^{-4}, B_o is 1.846×10^{-9}. And in terms of the Eq. (5), mean pore radius, r, is 0.173 μm, and the effective porosity, $(\varepsilon/\tau\cdot\delta)$, is 1.99×10^{4} m^{-1}.

Similarly, for the other eight type membranes, the respective values of A_o, B_o, r and $(\varepsilon/\tau\cdot\delta)$ can also be obtained, and the results are listed in Table 2. The determined pore sizes of PTFE 1.00, PVDF 0.45, PVDF 1.00, and PP 1.00 membranes are almost the same as the pore size given by the manufacturer, while the pore sizes of PTFE 0.22, PTFE 0.45, PVDF 0.22, PP 0.22 and PP 0.45 membranes are higher than that provided by the manufacturer. This may be due to different production methods and different process conditions. The increase in pressure difference makes a membrane with constant polymer volume become thinner, which leads to a decrease in porosity and pore size. The values of $(\varepsilon/\tau\cdot\delta)$ are in the range of 4,220 to 27,700 m^{-1}. In MD studies, a value of 2 is frequently assumed for tortuosity factor. The effective thickness of the membranes was calculated and found to be within the range of 20-80 μm.

1-2. Membrane Porosity, Contact Angle and LEP

Table 3 shows the values of density, porosity, CA and LEP for the various membranes. For same material membranes, bigger pore size membrane shows lower density and higher porosity. In general, the MD membrane porosity lies between 40 and 90%, and it is agreed upon that higher membrane porosity results in higher permeate flux [27]. Three types of PTFE membranes obtained approximately 80% porosity higher than the other six types of membranes.

Table 3. Measured and calculated properties of membranes

Membrane	Density (kg/m^3)	Porosity (%)	Contact angle (°)	LEP (kPa)
PTFE0.22	423.7	80	121±10	121.3±2.5
PTFE0.45	407.6	81	12±10	81.1±2.5
PTFE1.00	396.7	82	123±10	71.4±2.5
PVDF0.22	622.3	64	68±10	58±2.5
PVDF0.45	611.3	66	81±10	47.5±2.5
PVDF1.00	482.5	72	84±10	22.5±2.5
PP0.22	427.1	55	116±10	27.5±2.5
PP0.45	336.0	64	120±10	16.5±1
PP1.00	270.8	72	120±10	6±1

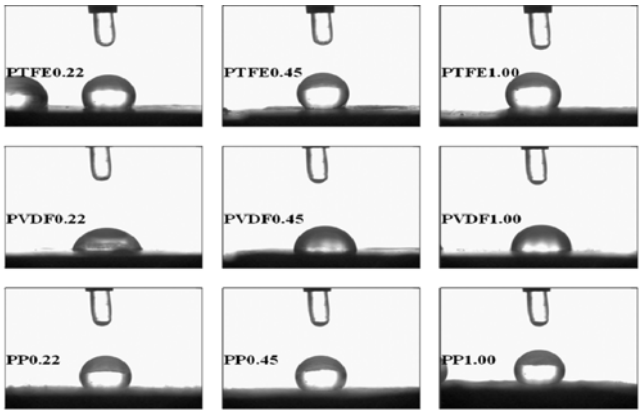

Fig. 5. Contact angle images of different membranes.

It must be pointed out that membranes with higher porosity exhibit lower thermal conductivity since the thermal conductivity of the gases entrapped within the membrane pores is an order of magnitude smaller than that of the hydrophobic polymer used for membrane preparation [28]. The SEM image of contact angle measurement on the different membrane surfaces is shown in Fig. 5. Agreeing with the values in Table 2, the contact angles of PVDF membranes were even lower than 90°, while the PTFE and PP material membranes showed higher values of approximately 120°. For MD membrane, the contact angle should be higher than 90°, so the PVDF membranes were not suitable for the MD process. The LEP values of PTFE membranes are higher than others. Specifically for the PTFE 0.22 membrane, if the feed side interface pressure is lower than 121.3 kPa, this will completely prevent pore wetting under a high concentration condition (20% NaCl). Besides, the membranes with bigger pore size show lower LEP values for same material membranes.

From the results of membrane porosity, gas permeability, and

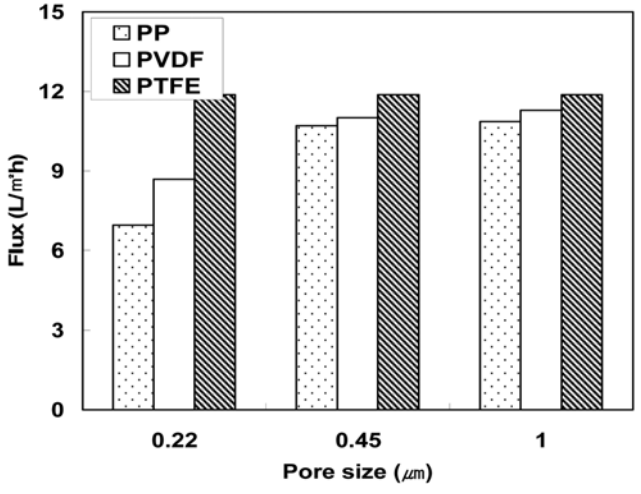

Fig. 6. Comparison of permeate flux for different membranes (Feed temperature of 80 °C; Feed flow rate of 250 ml/min; NaCl concentration of 3.5%; Coolant temperature of 15 °C; Coolant flow rate of 100 ml/min; Air gap thickness of 1 mm; Horizontal counter-current; The point part represents PP membranes, the blank part represents PVDF membranes, and the oblique line part represents PTFE membranes).

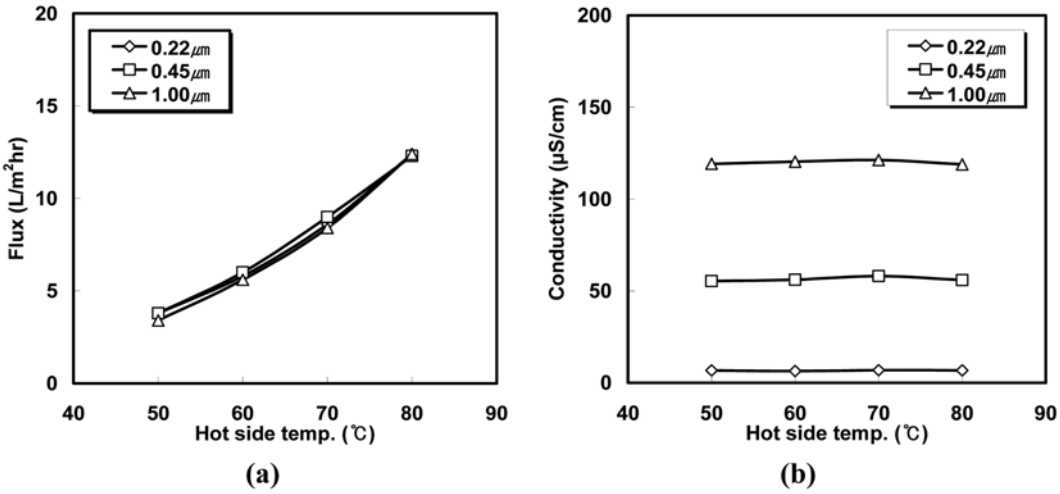

Fig. 7. Effect of hot side temperature on permeate flux (a) and conductivity (b) for different PTFE membranes (Feed flow rate of 250 ml/min; NaCl concentration of 3.5%; Coolant temperature of 15 °C; Coolant flow rate of 100 ml/min; Air gap thickness of 1 mm; Horizontal counter-current).

hydrophobicity for nine types of membrane, the PTFE 0.22, PTFE 0.45, and PTFE 1.00 membranes show more suitable for MD process than other six types of membranes for the higher porosity of 80%, and high hydrophobicity for contact angle of 120°, LEP of higher than 70 kPa.

2. Comparison of Nine Types of Membranes on Flux and Salt Rejection

Fig. 6 compares the permeate flux of nine types membranes made by PTFE, PVDF and PP materials, tested for AGMD performance under the same operating conditions: feed temperature of 80 °C; feed flow rate of 250 ml/min; NaCl concentration of 3.5%; coolant temperature of 15 °C; coolant flow rate of 100 ml/min; air gap thickness of 1 mm; and counter-current flow mode. In general, the permeate fluxes of membranes with higher porosity were higher than membranes with lower porosity (PTFE 0.22≈PTFE 0.45≈PTFE 1.00; PVDF 0.22<PVDF 0.45<PVDF 1.00; PP 0.22<PVDF 0.45< PVDF 1.00). The results also showed that the permeate fluxes for PTFE membranes were all higher than those obtained with PVDF and PP membranes under the different pore size conditions. For pore size 0.22 μm membranes, the permeate flux of PTFE was 37% higher than PVDF membrane, and 71% higher than PP membrane. For pore size 0.45 μm and the 1.00 μm membrane, the permeate flux of PTFE membranes is also higher than PP and PVDF membranes.

Another observation from comparing the membrane types was made by the result of membrane salt rejection. The salt rejections of PVDF membranes were in the range of 80% to 98%, lower than PTFE and PP membranes. This phenomenon is attributed to the inhomogeneous pore size distribution, and the PVDF membranes were wetted under experimental conditions. The explanation was proved by contact angles and LEP result. The contact angle of PVDF membranes are lower than 90°.

Because the salt rejection is higher than 99.8% and the permeate flux is higher than other two types of membranes, PTFE membranes were considered to be used in the next stage experiments to investigate the effect of operating variables. The PVDF and PP membranes were considered improper for the AGMD process. The experimental results agree with the membrane characterization results.

3. Comparison of Different PTFE Membranes

3-1. Effect of Hot Side Temperature on Permeate Flux and Conductivity

Fig. 7(a) compares the permeate flux for different pore sizes of PTFE membranes at a series of different hot side inlet temperatures under the same conditions: feed flow rate of 250 ml/min; NaCl concentration of 3.5%; coolant temperature of 15 °C; coolant flow rate of 100 ml/min; air gap thickness of 1 mm; and counter-current flow mode. The permeation flux increased with an increase in hot side inlet temperature. It is widely understood that a temperature difference across an MD membrane will induce water vapor to pass and some amount of permeate to be generated. Furthermore, a developing significant temperature difference should lead to greater desalination production rates. Besides, the permeate flux shows not much difference between the different pore size membranes. Fig. 7(b) compares the permeate conductivity of different membranes under the same conditions. The permeation conductivity keeps constant with the increase of hot side temperature. This phenomenon is an indication the temperature has no influence on the membrane pore wetting process.

3-2. Effect of Hot Side Flow Rate on Permeate Flux and Conductivity

Fig. 8(a) displays the effect of the hot side flow rate on the permeation flux for different membranes at the constant conditions: feed temperature of 80 °C, NaCl concentration of 3.5%, coolant temperature of 15 °C, and coolant flow rate of 100 ml/min. The permeation flux increased linearly when the feed flow rate increased from 100 ml/min to 400 ml/min for all membranes. Almost the same flux values were determined for the three membranes. Fig. 8(b) shows the effect of the hot side flow rate on the permeate conductivity for different membranes. The permeation conductivity increased with the increased flow rate for PTFE 0.45 and PTFE 1.00 membranes. The limited values were considered as the permeate conductivity values. This can be attributed to pressure variation at the flow rate, which may have allowed wetting to occur under fluctuating pressures at high flow rate. Once a pore had been penetrated, the mem-

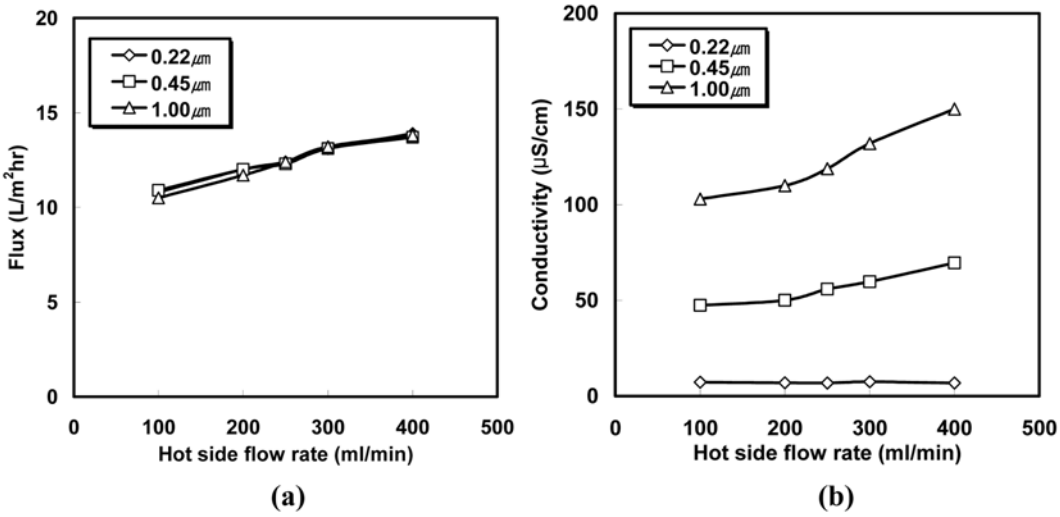

Fig. 8. Effect of hot side flow rate on permeate flux (a) and conductivity (b) for different PTFE membranes (Feed temperature of 80 °C; NaCl concentration of 3.5%; Coolant temperature of 15 °C; Coolant flow rate of 100 ml/min; Air gap thickness of 1 mm; Horizontal counter-current).

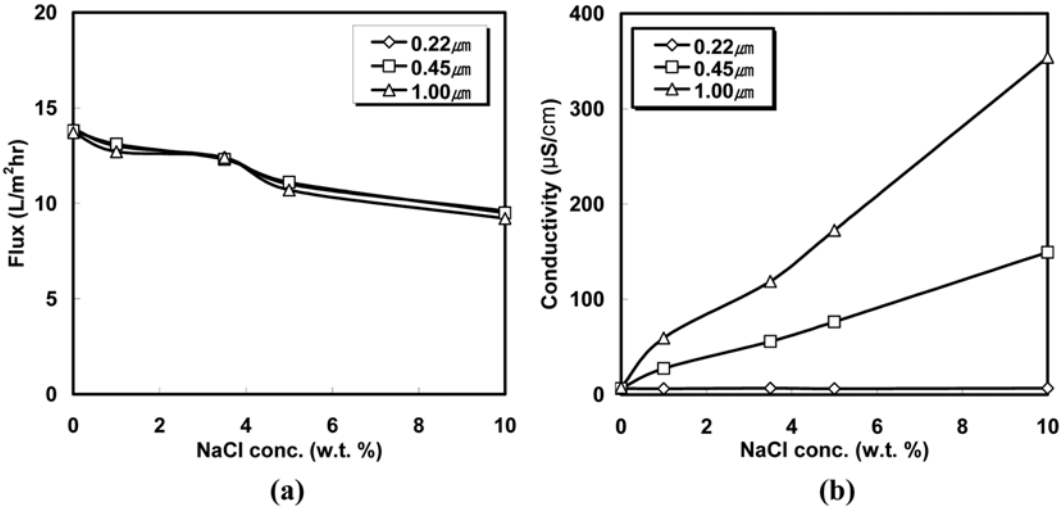

Fig. 9. Effect of NaCl concentration on permeate flux (a) and conductivity (b) for different PTFE membranes (Feed temperature of 80 °C; feed flow rate of 250 ml/min; Coolant temperature of 15 °C; Coolant flow rate of 100 ml/min; Air gap thickness of 1 mm; Horizontal counter-current).

brane was completely cleaned and dried before it was used again. And the permeate conductivity results agree with the LEP test results: PTFE 0.22 membrane showed higher hydrophobicity than other membranes. The conductivity of PTFE 0.22 membrane always stayed constant under 7 mS/cm showed no wetting occurred.

3-3. Effect of NaCl Concentration on Permeate Flux and Conductivity

Fig. 9(a) shows the relationship between the permeation flux and the NaCl concentration. The permeation flux slightly decreased when the feed NaCl concentration was increased from 1 to 10 wt%. The flux reduction can be attributed to the fact that the higher the concentration of NaCl solution, the higher the boiling point. The decrease of vapor pressure is believed to play an important role. This indicates that less vaporization of water occurs at the membrane surface causing a decrease in the amount of vapor flows through the membrane [29]. Vapor reduction occurs due to the salt concentration caused by the water activity, and the boundary layer mass and heat transfer coefficients decrease. This decrease can be reduced if the membrane module has minimum polarization. Schneider et al. have also found similar results from the effect of marginal feed concentration on the permeation flux and quality [30]. Fig. 9(b) shows the effect of NaCl concentration on permeation conductivity for different pore size membranes. The permeation conductivity increased rapidly with the increasing NaCl concentration for 1.00 μm membrane and 0.45 μm membrane but kept constant for pore size 0.22 μm membrane. The increase in the permeate conductivity was due to the decrease of LEP under higher concentration conditions.

From the results of Figs. 7, 8 and 9, almost the same permeate flux values were observed for different pore size membranes under the same operating conditions. For PTFE 0.45 and PTFE 1.00 mem-

branes, the permeation conductivity increased at high flow rate and high feed concentration conditions. The conductivity of the permeate remains invariable around 5-7 mS/cm for PTFE 0.22 membrane, which can provide high quality fresh water. The production rate for drinkable water of the unit was achieved around 12.5 L/m^{2}hr at feed temperature 80 ºC, feed flow rate of 250 ml/min and coolant temperature 15 ºC, coolant flow rate of 100 ml/min. We consider PTFE 0.22 membrane is much more suitable for the MD process than other membranes.

4. Effect of Temperature and Flow Rate on Mass Transfer Coefficient

The driving force for mass transfer across the membrane is the water vapor pressure difference between feed and permeate side. According to the Soret effect, not only a pressure difference but also a temperature difference induces mass transfer across the membrane. However, the thermal diffusion contribution is negligible in the MD.

Schofield's model and Dusty-Gas model are widely used for determining the mass transfer in the MD. Both models suggest that mass transfer rate is proportional to the vapor pressure difference across the membrane [31]

$$N=C\,\Delta p_{w,\,surface} \quad (6)$$

Where, N is the water vapor flux in L/m^{2}s, $\Delta p_{w,\,surface}$ is the water vapor pressure difference between feed and permeate side, which P can be calculated with Antoine equation: P=Exp(23.1964–(3816.44/(T+227.02))). C is the mass transfer coefficient that can be obtained experimentally (L/m^{2}s·Pa).

Fig. 10(a) represents the mass transfer coefficient vs. hot side flow rate between the feed temperature solution and condensate plate for three types of PTFE membranes. The mass transfer coefficient increased linearly with the increasing flow rate. That was due to the temperature polarization existing in the real running. Increasing the feed flow rate will reduce the boundary layer thickness when the Reynolds number increases. Fig. 10(b) shows mass transfer coefficient vs. hot side temperature for PTFE membranes. The mass transfer coefficient decreased linearly with increasing temperature. Decreasing the temperature difference causes a decrease in the vapors as well as the fraction of air, and thus increases the mass transfer coefficient. Besides, the mass transfer coefficient shows not much difference between the three membranes. Many researchers have reported the mass transfer coefficient for air gap MD in the range of 3×10^{-7} to 7×10^{-7} L/m^{2}s·Pa. However, we observed values from 1×10^{-7} to 1.4×10^{-7} L/m^{2}s·Pa in our investigation. The mass coefficient depends not only on the temperature difference but also on the membrane material, its roughness and its pore size distribution [25].

CONCLUSION

Nine types of membranes were characterized to understand the membranes more comprehensively, including density, porosity, CA, LEP, and membrane average pore sizes. The results show that PTFE membranes are more suitable for MD process for high porosity and high hydrophobicity. An AGMD system was successfully applied for distillation of NaCl solution. The experiment results agree with the membrane characterization results. The PTFE material membranes showed higher permeate flux than PVDF and PP membranes, and almost 100% salt rejection. Different pore size PTFE membranes showed similar permeate flux for all of the experiment conditions. The permeation flux increased with the increasing feed temperature and feed flow rate but decreased with the increasing concentration of NaCl in the feed solution. But the membrane difference did influence the conductivity for different flow rate and feed concentration conditions. The permeation conductivity remained constant with the increase of hot side temperature. But for PTFE 0.45 and PTFE 1.00 membranes, the permeation conductivity increased with the increasing NaCl concentration and feed flow rate. The conductivity remained invariable around 5-7 mS/cm for PTFE 0.22 membrane under all the conditions. The mass transfer coefficient increased slightly with the increasing hot side flow rate but decreased with the increasing hot side temperature obtained at the range of 1-1.4×10^{-7} L/m^{2}s·Pa.

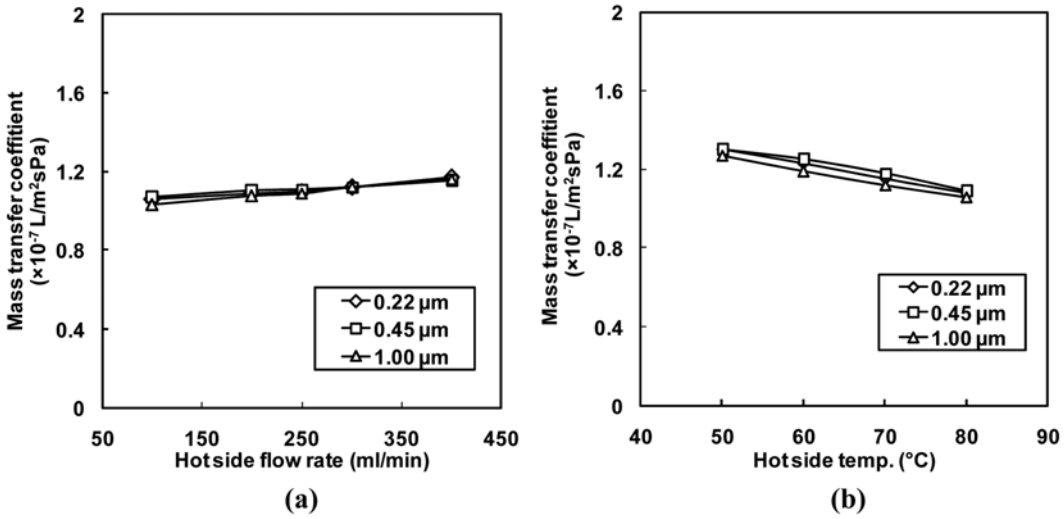

Fig. 10. Mass transfer coefficient as a function of the hot side flow rate (a) and hot side temperature (b) for PTFE membranes (Feed temperature of 80 ºC; NaCl concentration of 3.5%; Coolant temperature of 15 ºC; Coolant flow rate of 100 ml/min; Air gap thickness of 1 mm; Horizontal counter-current).

ACKNOWLEDGEMENT

This research was supported by a grant (07 SEAHERO B01-04-02) from the plant technology advancement program funded by the Ministry of Construction & Transportation of the Korean government. Research was partially performed as part of the project by the Ministry of Commerce, Industry and Energy (MOCIE) through the Regional Innovation Centre (RIC).

NOMENCLATURE

C : mass transfer coefficient
M : molecular weight of the gas
m : weight of membrane
N : water vapor flux
P : vapor pressure
P_m : pressure of membrane
R : gas constant
T : temperature
r : membrane pore radius
r_{max} : the largest pore radius
v : volume
X : geometric factor determined by pore structure
Δp : vapor pressure difference
σ : surface tension of the liquid
θ : liquid-solid contact angle
ε : membrane porosity
τ : membrane tortuosity
δ : membrane thickness
ρ : density

REFERENCES

1. S. A. Kalogirou, *Energy Combust. Sci*., **31**, 242 (2005).
2. A. Lamei, P. Van der Zaag and E. von Munch, *Energy Policy*, **36**, 1748 (2008).
3. K. W. Lawson and D. R. Lloyd, *J. Membr. Sci*., **124**, 1 (1997).
4. M. Gryta, A. W. Morawski and M. Tomaszewska, *Catal. Today*, **56**, 159 (2000).
5. L. Martinez-Diez and F. J. Florido-Diaz, *Desalination*, **137**, 267 (2001).
6. S. Nene, S. Kaur, K. Sumod, B. Joshi and K. S. M. S. Raghavarao, *Desalination*, **147**, 157 (2002).
7. A. Banat and J. Simandl, *J. Membr. Sci*., **163**, 333 (1993).
8. M. Gryta, M. Tomaszewska, J. Grzechulska and A. W. Morawski, *J. Membr. Sci*., **181**, 279 (2001).
9. H. Udriot, A. Araque and U. Von Stokar, *Chem. Eng. J*., **54**, 87 (1994).
10. M. Tomaszewska, M. Gryta and A. W. Morawski, *Sci*., **102**, 113 (1995).
11. R. Thiruvenkatachari, M. Matheswaran, T. O. Kwon, I. S. Moon and J. W. Kim, *Sep. Sci. Technol*., **41**, 3187 (2006).
12. M. Matheswaran, T. O. Kwon, J. W. Kim and I. S. Moon, *J. Ind. Eng. Chem*., **13**, 965 (2007).
13. J. W. Kim, S. E. Park, T.-S. Kim, D.-Y. Jeong and K.-H. Ko, *Nukleonika*, **49**, 137 (2004).
14. K. He, H. J. Hwang, M. W. Woo, I. S. Moon, *J. Ind. Eng. Chem*., DOI:0.1016/j.jiec.2010.10.007 (2010).
15. A. S. Jonsson, R. Wimmerstedt and A. C. Harrysson, *Desalination*, **56**, 237 (1985).
16. G. L. Liu, C. Zhu, C. S. Cheung and C. W. Leung, *Heat Mass Transfer*, **34**, 329 (1998).
17. A. Fahmi, Abu Al-Rub, Fawzi Banat and Khalid Bani-Melhem, *Sci. Technol*., **38**, 3645 (2003).
18. J. H. Hanemaaijer, *Memstill®, Desalination*, **168**, 355 (2004).
19. A. El Amali, S. Bouguecha and M. Maalej, *Desalination*, **168**, 357 (2004).
20. M. N. Chemyshov, G. W. Meindersma and A. B. de Haan, *Desalination*, **157**, 315 (2003).
21. J. Walton, H. Lu, C. Turner, S. Solis and H. Hein, Solar and water heat desalination by membrane distillation, desalination and water purification research and development program report No. 81, College of Engineering, University of Texas at El Paso (2004).
22. C. Bier and U. Plantikow, Solar powered desalination by membrane distillation, IDA World congress on desalination and water science, Abu Dhabi (1995).
23. G. W. Meindersma, C. M. Guijt and A. B. de Haan, *Desalination*, **187**, 291 (2007).
24. C. Feng, K. C. Khulbe, T. Matsuura, R. Gopal, S. Kaur, S. Ramakrishna and M. Khayet, *J. Membr. Sci*., **311**, 1 (2008).
25. R. Chouikh, S. Bouguecha and M. Dhahbi, *Desalination*, **181**, 257 (2005).
26. M. C. Garci-Payo, M. A. lzquierdo-Gill and C. Fernandez-Pineda, *J. Membr. Sci*., **169**, 61 (2000).
27. L. Palacio, P. Prádanos, J. I. Calvo and A. Hernández, *Thin Solid Films*, **348**, 22 (1999).
28. M. S. El-Bourawi, Z. Ding, R. Ma and M. Khayet, *J. Membr. Sci.*, **285**, 4 (2006).
29. Kevin W. Lawson and Douglas R. Lloyd, *J. Membr. Sci.*, **124**, 1 (1997).
30. S. Bouguecha and M. Dhahbi, *Desalination*, **152**, 237 (2002).
31. L. Gazagnes, S. Cerneaux, M. Persin, E. Prouzet and A. Larbot, *Desalination*, **217**, 260 (2007).
32. R. W. Schofield, A. G. Fane, C. J. D. Fell and R. Macoun, *Desalination*, **77**, 279 (1990).